© EARSeL and Warsaw University, Warsaw 2005. *Proceedings of 4th EARSeL Workshop on Imaging Spectroscopy. New quality in environmental studies*. Zagajewski B., Sobczak M., Wrzesień M., (eds)

SPATIAL ENHANCEMENT OF TIR ASTER DATA VIA VNIR IMAGES AND GENERALIZED LAPLACIAN DECOMPOSITION

Bruno Aiazzi[1], Stefano Baronti[1], Andrea Garzelli[2], Leonardo Santurri[1], Massimo Selva[1]

1. Institute of Applied Physics "Nello Carrara", IFAC-CNR, Firenze, Italy, surname@ifac.cnr.it
2. Department of Information Engineering, University of Siena, Siena, Italy, garzelli@dii.unisi.it

ABSTRACT

Image fusion aims at the exploitation of the information conveyed by data acquired by different imaging sensors. A notable application is merging images acquired from space by panchromatic and multi- or hyper-spectral sensors that exhibit complementary spatial and spectral resolution. Multiresolution analysis has been recognized efficient for image fusion. The *Generalized Laplacian Pyramid* (GLP), in particular, has been proven as the most efficient scheme due to its capability of managing images whose scale ratios are fractional numbers (non-dyadic data) and to its simple and easy implementation. Data merge based on multiresolution analysis, however, requires the definition of a model establishing how the missing spatial details to be injected into the multi-spectral bands are extracted from the panchromatic image. The model can be global over the whole image or depend on the local space-spectral context. This paper reports results on the fusion of *Advanced Spaceborne Thermal Emission and Reflection Radiometer* (ASTER) data. Each of the five thermal infrared (TIR) images (90m) is merged with the most correlated visible-near infrared (VNIR) image (15m). Due to the 6:1 scale ratio, the GLP has been utilized. The injection of spatial details has been ruled by means of the *Spectral Distortion Minimizing* (SDM) model that minimises the spectral distortion between the resampled and fused images. Notwithstanding the lack of a spectral overlap between the VNIR and the TIR bands, experimental results show that the fused images keep their spectral characteristics while the spatial resolution is enhanced.

INTRODUCTION

Space-borne imaging sensors allow data acquisition of the Earth surface on a routine basis. Multispectral (MS) observations, however, exhibit ground resolutions that may be inadequate to specific identification tasks. As in the case of satellite imagers like Ikonos, QuickBird and SPOT 5, which make available very high resolution MS and panchromatic (P) data, image fusion can be conceived also for ASTER TIR data, whose resolution is not sufficient for many application tasks: the VNIR ASTER bands could be the source of the enhancing spatial details.

Data fusion techniques take advantage of the complementary spatial/spectral resolution characteristics of imaging sensors to spatially enhance the acquired images. This specific aspect of data fusion is often referred to as *data merge* (i) or *band sharpening* (ii). In fact, in the case of P and MS data, the P band is acquired with the maximum resolution allowed by the sensor, while the MS bands are usually acquired at a coarser resolution, typically, two or four times lower. Once received, the P image may be merged with the MS images to enhance their spatial resolution.

Since the pioneering high-pass filtering (HPF) technique (iii), fusion methods based on injecting high-frequency components into resampled versions of the MS data have demonstrated a superior performance (iv). HPF basically consists of an addition of spatial details, into a bicubically-resampled version of the low-resolution MS image. Such details are obtained as the difference between the P image and its low-pass version achieved through a simple local pixel averaging. Later efforts take advantage from an underlying multiresolution analysis, by employing the discrete wavelet transform (DWT) (v), rational filter banks (vi), Laplacian pyramids (LP) (vii) and morphological pyramids (viii). Although seldom explicitly addressed by most of the literature, the rationale of high-pass detail injection as a spatial frequency spectrum substitution was formally developed in a multiresolution framework as an outcome of filter-banks theory (ix).

The DWT has been widely employed for remote sensing data fusion (x). According to the basic DWT merging scheme (xi), couples of sub-bands of corresponding frequency content are combined together. The merged image is synthesised by taking the inverse transform. Schemes based on the "à trous" wavelet algorithm were also recently proposed (xii,xiii). Unlike the DWT, which is critically sub-sampled, the "à trous" wavelet and the LP are over-sampled. The miss of the decimation step allows an image to be decomposed into nearly disjointed band-pass channels in the spatial frequency domain, without losing the spatial connectivity of its high-pass details, i.e. edges and textures. Starting from a synthetic yet comprehensive review of wavelet analysis, advantages for image merging of *redundant* multiresolution decompositions have been recently demonstrated (xiv). Advantages are found also for already established data fusion approaches once formulated in an undecimated multiresolution framework (xv). Furthermore, the LP can be easily generalised (GLP) to deal with scales whose ratios are whatsoever integer or even fractional numbers (vi).

Data fusion (merge) based on multiresolution analysis, however, requires the definition of a model describing how the missing high-pass information to be injected into the resampled MS bands is extracted from the P band (iv). The model can be global over the whole image or depend on local context, either spectral (xvi,xvii), or jointly spectral and spatial (xiv,xviii). The goal is to obtain fused bands as similar as possible to what the MS sensor would image at the resolution of the P band.

Preservation of spectral information, regarded as changes across spectral bands, or equivalently as colour hues in the composite representation of three bands at time, must be guaranteed after spatial enhancement. Hence, methods were developed based on the following steps: (a) transformation of the spectral bands, resampled at the scale of the P image, into Intensity-Hue-Saturation (IHS) coordinates, (b) replacement of the *smooth* I component with the *sharp* P image, (c) inverse transformation to the original spectral domain. IHS fusion methods (xix), however, may introduce severe radiometric distortions (e.g. bias in local mean) in the sharpened MS bands, due to the low-pass component of the P image that affects the fused product. To overcome such inconveniences, IHS fusion was either extended into a multiresolution framework (only details of the I component are replaced with those of P) (xii,xiii), or analogously the smooth I component was sharpened by modulating each pixel by the ratio of P to its low-pass version (xx). The latter procedure may introduce radiometric inaccuracies in textured areas, due to statistical instabilities and the bias of the rational term. All the above methods are used in the case of exactly three spectral bands. When the number of components is larger, IHS methods are applied to three bands at a time.

Although IHS-based methods were specifically developed to preserve spectral information, the problem of spectral distortion was never explicitly considered, when the injection model was set-up. Spectral distortion can be measured, regardless of the number of spectral components, as the absolute angle between a pixel vector in the true and in the fused MS data. Such an angle should be lower than or equal to that measured between the expanded original low-resolution MS data and the true high-resolution MS data, when available (e.g. in simulation carried out on spatially degraded images). The case of equality means that the fusion algorithm has preserved the available spectral information (SDM model) with the benefit of a spatial enhancement.

In this work, the GLP fusion scheme (vii) is utilized for the fusion of TIR ASTER images by injecting spatial details extracted from VNIR bands, the injection being ruled by the SDM model. After reporting the definition of GLP, several fusion models embedded in the GLP scheme are reported. ASTER data characteristics are then examined in order to adapt the fusion algorithm to such data. Results are then reported and discussed. Eventually, conclusions are drawn.

GENERALISED LAPLACIAN PYRAMID

The Laplacian pyramid (LP) is derived from the Gaussian pyramid (GP), which is a sequence of multiresolution approximations obtained through a recursive *reduction* of the image data set. Reduction by *2* (*reduce$_2$(.)*) consists of separable low-pass filtering followed by decimation by 2 along rows and columns. The 2-D low-pass reduction filter is generally with null phase (xxi). If $G_0(m,n)$ is the original grey-scale image, the GP is iteratively defined as

$$G_k(m,n) = reduce_2[G_{k-1}](m,n)$$

in which *k* identifies the level of the pyramid, *K* being the top level (approximation). From the GP, the *enhanced* LP (ELP) (xxi) is defined as

$$L_k(m,n) = G_k(m,n) - expand_2[G_{k+1}](m,n)$$

in which $expand_2[G_{k+1}]$ denotes the (*k+1*)-th GP level expanded by 2 to match the size of the underlying *k*-th level. The 2-D low-pass filter used for expansion is still separable and zero-phase; it must cut-off at one half of the signal band-width to exactly reject the spectral images introduced when samples are zero-interleaved. The base-band approximation is gathered with the band-pass ELP, i.e. $L_K(m,n) = G_K(m,n)$, to yield a complete image description comprising both low-pass approximation and band-pass details. An octave (E)LP is oversampled by a factor *4/3* at most (when the base-band is one pixel wide). Computational overhead is kept moderate thanks to the decimation of the low-pass components. Figure 1 displays examples of GP and ELP of a Landsat image (TM Band 5). The former is a sequence of frequency-octave low-pass approximations; the latter is a sequence of octave band-pass details (zero-mean) plus the base-band approximation.

When the scale ratio is not a power of *2*, but any positive integer or fractional number, the operators *reduce$_2$*(.) and *expand$_2$*(.) are *generalised* to deal with fractional reduction and expansion (vii).

Reduction by an integer *p* (*p > 1*), *reduce$_p$(.),* consists of separable low-pass filtering followed by decimation by *p* along rows and columns. The 2-D low-pass reduction filter is with null phase (xiv) and has a *3* dB frequency cut-off at *1/p*. Expansion by an integer *q*, expand$_q$(.), means up sampling by *q* (interleave couples of adjacent samples with *q-1* zeroes) followed by low-pass filtering.

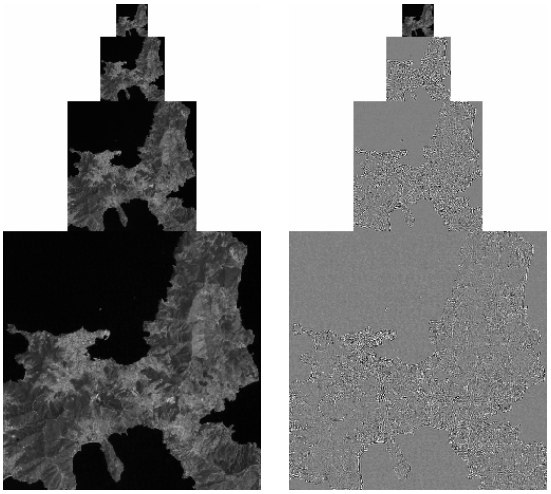

Figure 1: GP (left) and ELP (right) with scale ratio equal to 2.

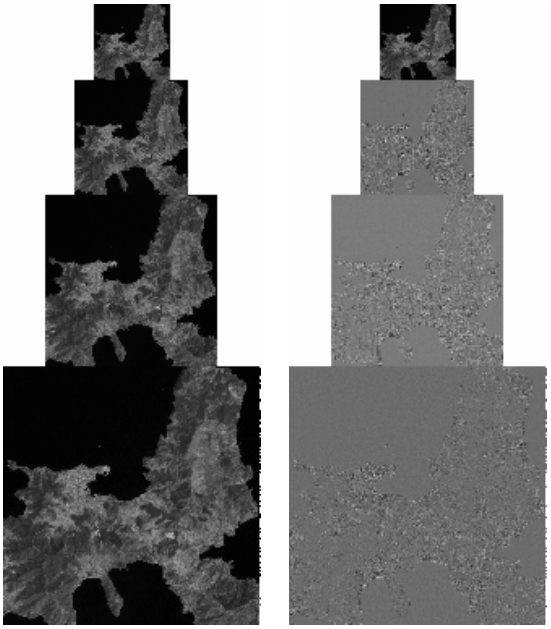

Figure 2: GGP (left) and GLP (right) with scale ratio p/q=3/2.

The 2-D low-pass filter for expansion is still separable and zero-phase; it must cut-off at *1/q* of the signal bandwidth to exactly reject the spectral images introduced when samples are zero-interleaved. A *reduction* by *p/q* (*p* > *q*) is given by an expansion by *q* followed by a reduction by *p*:

$$reduce_{p/q}(.) = reduce_{p}[expand_{q}(.)].$$

An *expansion* by *p/q* (*p* > *q*) is obtained as an expansion by *p* followed by a reduction by *q*:

$$expand_{p/q}(.) = reduce_{q}[expand_{p}(.)].$$

If $G_0(m,n)$ is the original grey-scale image, the generalised GP (GGP) with fractional scale ratio *p/q* is defined as

$$G_k(m,n) = reduce_{p/q}[G_{k-1}](m,n).$$

The generalised (E)LP (GLP) (vii) is defined as

$$L_k(m,n) = G_k(m,n) - expand_{p/q}[reduce_{p/q}(G_k)](m,n).$$

Figure 2 displays examples of generalised GP (GGP) and GLP; the scale ratio is *3/2* (*p = 3, q = 2*). In the following all detail pyramids will be denoted as GLPs, irrespective of the scale ratio.

In the case *p = 2, q = 1,* corresponding to frequency octave decomposition, polynomial kernels with *3* (linear), *7* (cubic), *11* (fifth-order), *15* (seventh-order), *19* (ninth-order) and *23* (eleventh-order) coefficients (nicknamed *taps*) have been used (vi).

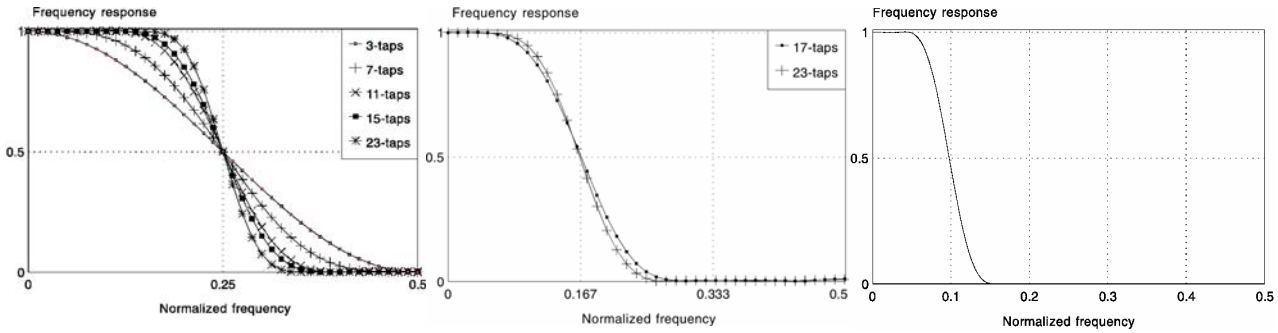

Figure 3: Frequency responses of GLP-generating filters, with cut-offs at one half (top), one third (centre) and one fifth (bottom). Such filters may be used for reduction and must be used for expansion (with properly adjusted DC gains).

The term *polynomial* stems from interpolation and denotes that filtering can be seen as fitting an *n*-th order polynomial to nonzero samples. The *7*-taps kernel is widespread to yield a separable bicubic interpolation. For $p = 3$, two kernels with *17* and *23* taps have been designed while for $p = 5$, a kernel with *29* coefficients has been derived. Frequency responses are plotted in Figure 3. The filter design stems from a trade-off between selectivity (sharp frequency cut-off) and computational cost (number of nonzero coefficients). The absence of ripple outside the pass band, which can be noticed in plots with logarithmic scale (xiv), is perhaps the most favourable characteristic.

Figure 4 shows the flowchart of sharpening of low-resolution MS bands via a high-resolution P image by means of the GLP for the general case of p/q scale ratio between data. Fractional scale ratios are feasible thanks to cascaded expansions and reductions by integer factors. Notice that for a p/q scale ratio, only *one* filter with $1/p$ cut-off is required. In fact, when reduction is cascaded to expansion, the low-pass filtering step is omitted after up sampling by q, as well as before down sampling by q in the expansion, by assuming a near ideal frequency cut-off for the filters.

As it appears from Figure 4, the injection model is always calculated between MS bands resampled to the final scale and the low-pass approximation of the P image. These data sets should have the same extent of spatial frequency content. This issue may be crucial in practical case, due to the presence of a non-ideal *modulation transfer function* (MTF) generally different from one band to another. In that case, the reduction filter only may be replaced with a kernel approximating the average MTF of the MS bands. The expansion filter, responsible for resampling of the data sets, is left unchanged and equals one of the prototypes in Figure 3.

DETAIL INJECTION MODELS

Detail injection models deal with the transformation of spatial structures changing between the different spectral bands. Specifically, they describe the relationships between the detail observed in the P image and the one that should appear in the enhanced MS band.

The simplest model is a global gain equalisation, which can be achieved either by preliminarily matching the histogram of the P image to that of each MS band, or equivalently by weighting the details to be injected into the l-th band with the ratio of *global* standard deviations of the l-th MS band and the low-pass approximation of the P image.

According to a local, i.e. space-varying, model, the details taken from the higher-resolution P image are selected and weighted by a space-varying factor, based on a statistical model. This was recently accomplished (xiv) by measuring the degree of matching between each of the expanded MS bands and the low-pass approximation of the P band.

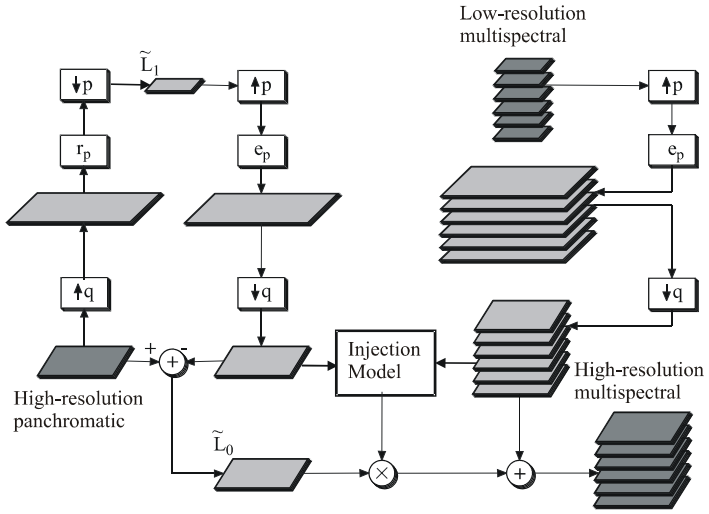

Figure 4: Flowchart of GLP-based Pan-sharpening for scale ratio equal to p/q (p>q). The up-samplers ↑ and down-samplers ↓, with the reduction r_p and expansion e_p filters build the GLP.

Let $L_0^P(m,n)$ be the high-resolution P details at level $k=0$ of the GLP. Let also $expand\{G_1^P\}(m,n)$ be the low-resolution approximation of the P image. Analogously, $expand\{G^{(l)}\}(m,n)$ denotes the l-th band of the MS image expanded to match the scale of the P image. The model establishes a local relationship between the resampled l-th band and the low-pass approximation of P, based on local statistics computed on a sliding window. Hereafter $\sigma_l(m,n)$ and $\sigma_P(m,n)$ are respectively the local standard deviations of $expand\{G^{(l)}\}(m,n)$ and $expand\{G_1^P\}(m,n)$, respectively, and $\rho(m,n)$ is their correlation coefficient (CC). Let also $0<\theta<1$ be a constant threshold set equal to the one's complement of the global CC ρ_{lP}; hence, the lower the correlation, the higher the threshold. The local weighting coefficient α_l, by which the detail $L_0^P(m,n)$ is multiplied before being added to $expand\{G^{(l)}\}(m,n)$, is clipped above three to avoid numerical instabilities and is given by:

$$\alpha_l = min[\sigma_l / (1+\sigma_P), 3] \text{ if } \rho \geq \theta$$
$$\alpha_l = 0 \quad \text{if } \rho < \theta.$$

Thus, *unmixing* of coarse MS pixels (xvi) may be achieved based on the local statistics of the P image, whose approximation yields the local gain adjustment and drives the matching criterion. The model yields a fusion scheme with a *context-based decision*.

A third model is the *spectral* information preserving injection model (xxii). It works with an arbitrary number of bands and requires neither calculation of local statistics nor thresholds and other adjustable parameters. The model allows detail injection into the spectral bands in such a way that the sharpened spectral pixel is a vector always parallel to the resampled low-resolution original spectral pixel. The following local weight is calculated at every pixel, for each band:

$$\alpha_l = expand[G^{(l)}](m,n) / expand[G_1^P](m,n). \quad (1)$$

It is easily verified (xxii) that the vector of detail components to be injected into the spatially resampled spectral pixel is always parallel to the resampled MS pixel itself. Hence, the sharpened spectral pixel vector is parallel to the resampled MS pixel vector and the spectral distortion of the fused product with the original MS image is zero. This model will be referred to in the following as *spectral distortion minimising* (SDM) and will adopted in the experiments.

ASTER DATA CHARACTERISTICS

Table 1 reports some of the main characteristics of ASTER data. Focusing on VNIR and TIR bands, it is apparent that the spatial resolution of VNIR images is 6 times higher than that of TIR ones and there is obviously no spectral overlap between VNIR and TIR bands. The data we have processed are L1B radiance at the sensor images, radiometrically corrected and georeferenced.

Table 1: Spectral,Spatial and radiometric resolution of ASTER data.

Characteristic And Spectral Range		
VNIR (15m – 8 bit/sample)	SWIR (30m – 8 bit/sample)	TIR (90m – 12 bit/sample)
Band 1: 0.52 - 0.60 μm	Band 4: 1.600 - 1.700 μm	Band 10: 8.125 - 8.475 μm
Band 2: 0.63 - 0.69 μm	Band 5: 2.145 - 2.185 μm	Band 11: 8.475 - 8.825 μm
Band 3: 0.76 - 0.86 μm	Band 6: 2.185 - 2.225 μm	Band 12: 8.925 - 9.275 μm
Band 3: 0.76 - 0.86 μm	Band 7: 2.235 - 2.285 μm	Band 13: 10.25 - 10.95 μm
	Band 8: 2.295 - 2.365 μm	Band 14: 10.95 - 11.65 μm
	Band 9: 2.360 - 2.430 μm	

FUSION BETWEEN VNIR AND SWIR ASTER DATA

Figure 5 reports the fusion scheme that has been adapted to cope with ASTER data. The 6:1 reduced VNIR image is obtained by means of the cascade of two reduction steps ($p_1=3$, $p_2=2$, respectively. The 6:1 expansion of the reduced VNIR and TIR images are instead performed by means of two expansion steps ($p_1=2$, $p_2=3$, respectively). SDM is the injection model in which α_l is selected according to eq. (1).

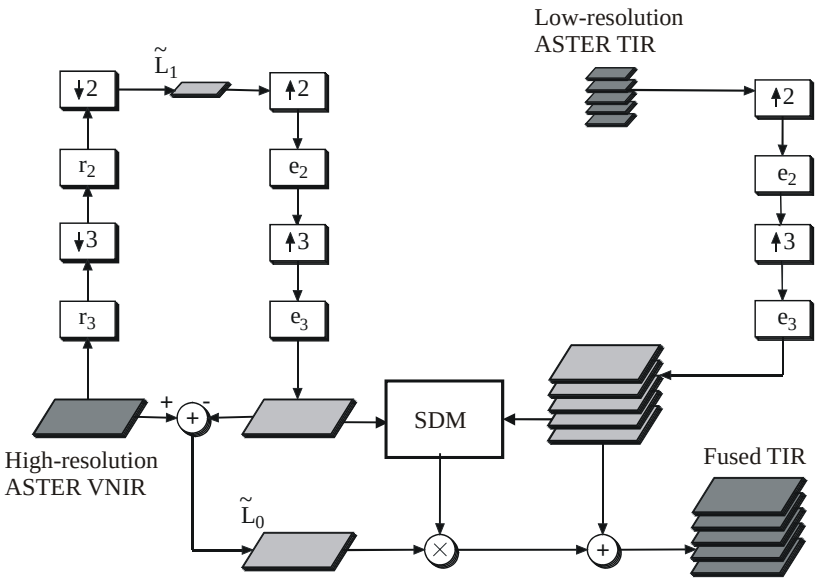

Figure 5: GLP-based Pan-sharpening for ASTER TIR-VNIR fusion. The scheme of figure 4 is modified taking into account that q=1 and that the p=6 reduction is obtained by the cascade of two reductions of factors $p_1=3$ and $p_2=2$. In the same way the p=6 expansion is obtained by the cascade of a $p_1=2$ and a $p_2=3$ expansion. The injection model is computed at the scale of the fused product between the low-pass approximations of VNIR and the expanded TIR bands.

RESULTS

The GLP-SDM fusion method has been experimented on the sample L1B data of ASTER imagery of Mt. Fuji made available by Earth Remote Sensing Data Analysis Center (ERSDAC) of Ministry of Economy, Trade and Industry of Japan (METI). The similarity of the images to be merged is crucial for the quality of the fusion process. In our work similarity has been assessed by means of the correlation matrix, which has been computed between the TIR and the reduced (6 times) VNIR bands and is reported in Table 2. The values over the diagonal refer to the whole image reported in Figure 6 while the values under the diagonal refer to the upper left quarter of Figure 6 and are not, thus, biased by the sea influence, whose effect is to increase the correlation values. The analysis of Table 2 reveals that VNIR band 2 is strongly correlated with all the TIR bands. Therefore it is the most suitable to originate the spatial details to be injected in the expanded TIR bands and such details will probably determine a fused image of good quality. In addition, as expected, all the TIR bands are extremely correlated to each other. The visual analysis of Figure 6 confirms that, apart from some difference in contrast, TIR band 10 is very similar to VNIR band 2 while strong differences exist with respect to VNIR band 3.

Table 2: Correlation between ASTER bands for the test image. A significant correlation exists between VNIR band 2 and all the TIR bands.

Band	1	2	3	10	11	12	13	14
1	1	0.8838	0.0645	0.6631	0.6625	0.6583	0.67318	0.6763
2	0.9353	1	0.4424	0.8911	0.8911	0.8872	0.8916	0.8924
3	-0.518	-0.263	1	0.5501	0.5569	0.5578	0.5318	0.5235
10	0.7118	0.8585	0.0279	1	0.9950	0.9939	0.9938	0.9920
11	0.7092	0.8563	0.0357	0.9949	1	0.9957	0.9940	0.9916
12	0.7048	0.8519	0.0449	0.993	0.9959	1	0.9939	0.9915
13	0.7251	0.8641	0.0116	0.9936	0.9942	0.9942	1	0.9970
14	0.7324	0.87	-0.002	0.9917	0.9918	0.9913	0.997	1

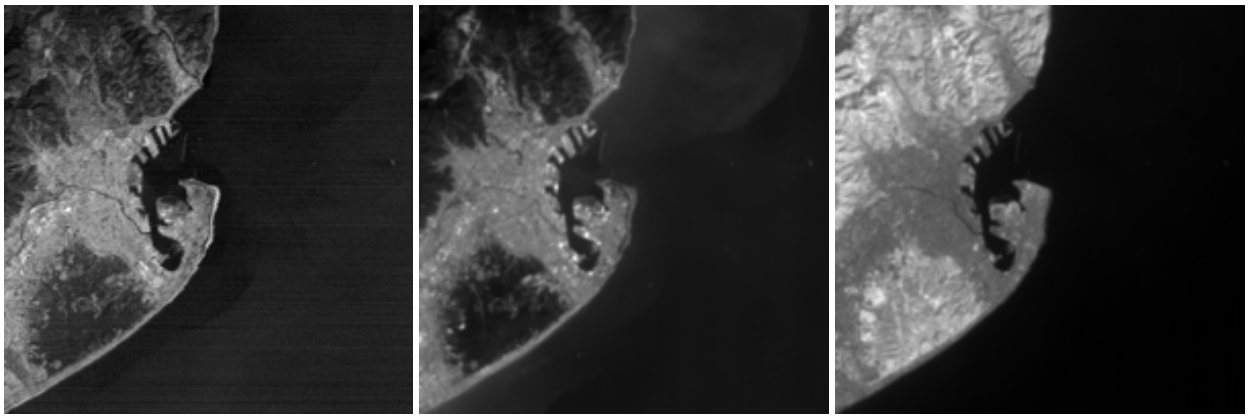

Figure 6: TIR B10 (left), VNIR B2 (centre) and B3 (right). VNIR bands have been reduced at the same scale of TIR ones by low-pass filtering and decimation.

Fusion results are reported in Figure 7. TIR bands 14, 12, and 10 have been represented in false colour on R, G, and B channels, respectively. The original 90m TIR image (left) has been expanded to the same scale of VNIR bands and can be compared with the TIR images fused by means of VNIR band 2 (centre) and 3 (right). As expected from the correlation analysis, the original

TIR image is more similar to the image fused by VNIR band 2. In particular, the fusion by VNIR band 3 suffers from an over-enhancement of vegetated areas that appear extremely textured, thus reflecting the response of vegetation in the VNIR channel. Notwithstanding the difference in contrast, all the images appear spectrally similar as a consequence of the fusion by the SDM model.

Concerning quantitative results, we investigated on the first property of the protocol reported in (iv): *for each band, the fused image is reduced to its original resolution and compared with the true image*. Results are reported in Table 3 and 4 for the fusion by means of VNIR band 2 and 3, respectively. Apart from the bias in the mean that is practically zero, results reported in Table 3 are better than those reported in Table 4. In fact, for each band, the difference in standard deviation and the mean square error (MSE) are lower in Table 3 than in Table 4, while the correlation is higher. Also the spectral angle mapper (SAM) has been computed to assess the spectral distortion of the fusion process. As expected, it was found practically zero in both cases (0.0334 and 0.0333 degree, respectively). It is important to evidence that the scores reported in Table 3 and 4 are absolute values and that they are low, notwithstanding the dynamic range of the TIR images is 12 bit.

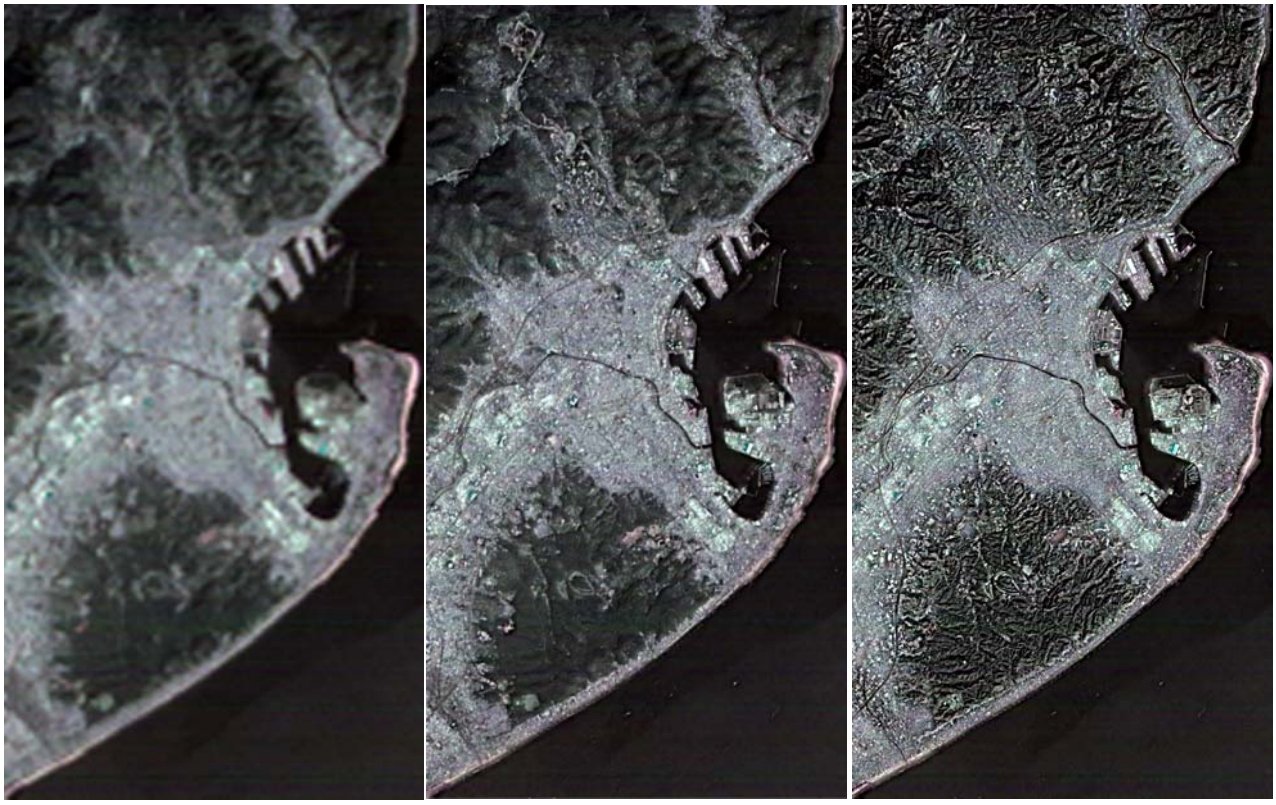

Figure 7: False colour composite pictures of TIR bands 14, 12, and 10 linked to R, G, and B channels, respectively: expanded TIR (left), fused TIR by VNIR band 2 (centre) and 3 (right).

Table 3: Score parameters computed on TIR bands fused by means of VNIR band 2.

TIR Band	Mean Bias	St. Dev. Bias	MSE	Correlation
10	0.0367	1.9652	135.4188	0.9789
11	0.0364	2.0378	154.9750	0.9800
12	0.0394	2.2453	172.1465	0.9774
13	0.0079	2.6443	239.3021	0.9745
14	0.0530	2.7816	251.5762	0.9703

Table 4: Score parameters computed on TIR bands fused by means of VNIR band 3.

TIR Band	Mean Bias	St. Dev. Bias	MSE	Correlation
10	0.0047	2.8453	276.3941	0.9576
11	0.0062	2.9680	314.3599	0.9601
12	0.0063	3.3885	352.2002	0.9548
13	0.0086	4.3424	512.3738	0.9471
14	0.0271	4.8563	559.6409	0.9368

CONCLUSIONS

The GLP scheme demonstrated its capability to merge images at any rational scale ratio, thus being superior to any dyadic wavelet scheme. In the case of 6:1 ASTER VNIR-TIR image fusion only the composition of two cascaded filters is needed for reduction and expansion. In addition, the adoption of the SDM injection model guarantees that the fused images have no spectral distortion with respect to the simply expanded images. This property can be particularly useful when, as in the ASTER case, no spectral overlap exists between the images that are to be merged. The analysis of correlation between bands is useful to find out the most suitable band from which to extract the spatial details to be injected. Further work should be devoted to investigate on practical applications of the proposed technique. Such a work should hopefully involve the user community on a representative test set.

ACKNOWLEDGEMENTS

The authors wish to thank ERSDAC/METI for providing the test data and Dr. Luciano Alparone for his valuable discussions on data fusion.

References

i Scheunders P & P De Backer, 2001. Fusion and merging of multispectral images with use of multiscale fundamental forms. Journal of the Optical Society of America A, 18(10): 2468-2477.

ii Vrabel J, 2000. Multispectral imagery advanced band sharpening study. Photogramm. Eng. Remote Sensing, 66(1): 73-79.

iii Chavez P S, S C Sides & J A Anderson, 1991. Comparison of three different methods to merge multi-resolution and multispectral data: Landsat TM and SPOT panchromatic. Photogramm. Eng. Remote Sensing, 57(3): 295-303.

iv Wald L, T Ranchin & M Mangolini, 1997. Fusion of satellite images of different spatial resolutions: assessing the quality of resulting images. Photogramm. Eng. Remote Sensing, 63(6): 691-699.

v Zhou J, D Civco & J Silander, 1998. A wavelet transform method to merge Landsat TM and SPOT Panchromatic data. International Journal of Remote Sensing, 19(4): 743-757.

vi Aiazzi B, L Alparone, F Argenti & S Baronti, 1999. Wavelet and pyramid techniques for multisensor data fusion: a performance comparison varying with scale ratios. In Image and Signal Processing for Remote Sensing V, (SPIE EUROPTO 3871, Firenze), 251-262.

vii Aiazzi B, L Alparone, S Baronti & R Carlà, 1998. An assessment of pyramid-based multisensor image data fusion. In Image and Signal Processing for Remote Sensing IV, (SPIE EUROPTO 3500, Barcelona), 237-247.

viii Flouzat G, O Amram, F Laporterie & S Cherchali, 2001. Multiresolution analysis and reconstruction by a morphological pyramid in the remote sensing of terrestrial surfaces. Signal Processing, 81(10): 2171-2185.

ix Argenti F & L Alparone, 2000. Filterbanks design for multisensor data fusion. IEEE Signal Processing Letters, 7(5): 100-103.

x Ranchin T & L Wald, 2000. Fusion of high spatial and spectral resolution images: the ARSIS concept and its implementation. Photogramm. Eng. and Remote Sensing, 66(1): 49-61.

xi Li H, B S Manjunath & S K Mitra, 1995. Multisensor image fusion using the wavelet transform. Graphical Models Image Processing, 57(3): 235-245.

xii Nuñez J, X Otazu, O Fors, A Prades, V Palà & R. Arbiol, 1999. Multiresolution-based Image fusion with additive wavelet decomposition. IEEE Trans. Geosci. Remote Sensing, 37(3): 1204-1211.

xiii Chibani Y & A Houacine, 2002. The joint use of IHS transform and redundant wavelet decomposition for fusing multispectral and panchromatic images. International Journal of Remote Sensing, 23(18): 3821-3833.

xiv Aiazzi B, L Alparone, S Baronti & A Garzelli, 2002. Context-driven fusion of high spatial and spectral resolution data based on oversampled multiresolution analysis. IEEE Trans. Geosci. Remote Sensing, 40(10): 2300–2312.

xv Ranchin T, B Aiazzi, L Alparone, S Baronti & L. Wald, 2003. Image fusion – the ARSIS concept and some successful implementation schemes. ISPRS J. Photogr. Remote Sensing, 58:4-18.

xvi Zhukov B, D Oertel, F Lanzl & G Reinhackel, 1999. Unmixing-based multisensor multiresolution image fusion. IEEE Trans. Geosci. Remote Sensing, 37, 3:1212-1226.

xvii Cornet Y, S De Béthune, M Binard, F Muller, G Legros & I Nadasdi, 2001. RS data fusion by local mean and variance matching algorithms: their respective efficiency in a complex urban context. In Proceedings of the IEEE/ISPRS joint Workshop on Remote Sensing and Data Fusion over Urban Areas (URBAN, Rome), 105-111.

xviii Hill J, C Diemer, O Stöver & T Udelhoven, 1999. A local correlation approach for the fusion of remote sensing data with different spatial resolutions in forestry applications. ISPRS International Archives of Photo-grammetry and Remote Sensing, 32(7, W6).

xix Carper W, T Lillesand & R Kiefer, 1990. The use of Intensity-Hue-Saturation transformations for merging SPOT panchromatic and multispectral image data. Photogramm. Eng. and Remote Sensing, 56(4): 459-467.

xx Liu J, 2000. Smoothing filter-based intensity modulation: a spectral preserve image fusion technique for improving spatial details. Int. Journal of Remote Sensing, 21(18):3461-3472.

xxi Aiazzi B, L Alparone, S Baronti & F Lotti, 1997. Lossless image compression by quantization feedback in a content-driven enhanced Laplacian pyramid. IEEE Trans. Image Processing, 6(6): 831-843.

xxii Aiazzi B, L Alparone, S Baronti, I Pippi & M Selva, 2002. Generalized Laplacian pyramid-based fusion of MS + P image data with spectral distortion minimization. ISPRS International Archives of Photogrammetry and Remote Sensing, 34(3B, W3): 3-6.